

## TECHNICAL PAPER

## STUDY ON DEEP DRAWING BEHAVIOR OF THE INTERSTITIAL FREE STEEL IN CORRELATION WITH THE MICROSTRUCTURE

*Mykhaylo Romanyuk<sup>1</sup>, Elena Brandaleze<sup>1</sup>*<sup>1</sup> *Process Technology, Metallurgy Department, DEYTEMA Centre, Universidad Tecnológica Nacional- Facultad Regional San Nicolás, Colón 332, San Nicolás, 2900, Argentina.*\*Corresponding author: [ebbrandaleze@frsn.utn.edu.ar](mailto:ebbrandaleze@frsn.utn.edu.ar), tel.: +54 336 4420830 211, Facultad Regional San Nicolás / Universidad Tecnológica Nacional, 2900, San Nicolás, Argentina.

Received: 09.02.2022

Accepted: 05.05.2022

## ABSTRACT

The Interstitial Free steels (IF) are widely used in the automotive industry due to their excellent mechanical properties (relative to deep drawing), combined with high mechanical strength. Currently, the main applications of the IF steel are focused on automotive industry parts production with a high forming requirement, such as the exterior panels of the cars body. The objective of this paper was to present results obtained about the behaviour of the IF steel sheets associated with high deformation. In order to evaluate the deep drawing aptitude of the sheet, samples were subjected to different mechanical tests: tensile test, hole expansion tests,  $n$  and  $r$  values determination and Erichsen test, all of them used commonly to verify the deep drawability of the sheets. This information was completed with microhardness measurements. The results were correlated with microstructural studies involving optical microscopy and scanning electron microscopy (SEM), including semi-quantitative EDS analysis. The IF steel microstructure is formed from ferritic grains with very fine grain size. Different types of precipitates are distributed on the grain boundaries and within grains. The information obtained allowed to understand the mechanical behavior in relation with the distribution of the particle's types (identified in the structure), their composition and impact on the microstructure evolution associated with temperature. Through thermodynamic simulation applying FactSage 8.1, the phase transformation temperature ( $T_{\gamma \rightarrow \alpha}$ ) and the conditions of precipitates formation were estimated, in order to correlate with industrial processing conditions of the material. In addition,  $T_{\gamma \rightarrow \alpha}$  value was determined by dilatometry test. The main precipitates identified in the microstructure were TiN, TiC, TiS and  $C_2S_2Ti_4$ , in coincidence with the results of the thermodynamic predictions. It is known that the failure of the material during the deep drawing or stamping process of the pieces is evidenced through the formation of microcracks or cracks in areas with changes of critical angles. For this reason, it is relevant to understand the mechanisms of fracture nucleation and propagation of the IF steel. In this sense, a fractography study was carried out on the samples tested by tensile test up to failure. It was possible to verify the presence of cavitation mechanism as results of super-plastic flow at high deformation conditions, promoting necking and fracture after a high plastic deformation achieved. All the results obtained allowed to verify that the IF steel sheet satisfy the requirements of an EDDQ quality steel.

**Keywords:** steel; deep drawability; microstructure; mechanical behaviour, fractography.

## INTRODUCTION

Steel is an essential material in the economy of industrially developed countries and presents special interest to achieve the growth of the automotive industry. The current demand for steels has critical requirements such as high mechanical strength and low weight, which promote passenger safety and fuel savings. These purposes are possible due to the possibility of forming sheets at room temperature to manufacture high-strength structural parts or panels with complex shapes. One of the manufacturing processes used for this type of auto parts is stamping. Currently ULC steel grades containing ultra-low carbon contents, such as the Interstitial Free (IF), are considered one of the material of great industrial interest for this type of applications due to their particular combination of mechanical properties: aptitude to deep drawing, acceptable values of mechanical resistance and a microstructure of ultrafine grain [1].

The mechanical properties can be improved by refining and re-arranging the microstructure. In addition, these materials can be easily coated, painted and welded. These properties make IF steel suitable to be applied to the exterior panels of the automotive body [2-4]. These steels are characterized by containing micro alloying elements such as titanium and/or niobium, among

other elements that remove the carbon from the matrix, promoting the precipitation of different carbides, nitrides and carbonitrides (of Ti and Nb). The precipitates affect the mechanical properties of steels because they control grain size refinement. In this steel grain shape is nearly equiaxed even when the strain is large. In addition, crystallographic texture represents another factor that influences the material drawability aptitude. Fibers  $\gamma$  {ND // <111>} are suitable for deep drawing, while the presence of  $\alpha$  fibers {RD // <110>} could adversely affect on the sheets forming [4, 5].

Different methods are used to evaluate the drawability of alloys through mechanical tests in order to obtain knowledge about the mentioned behaviour. It is relevant to consider that cold forming induces strength properties increase and inhomogeneous deformation, promoting residual stresses. These tests are classified into stretching tests, drawing tests and combined tests. Within the stretching tests, Erichsen test can be mentioned, which consists of the stretching of a circular steel sample through a hemispherical punch and where the height of the cup (or advance of the punch) is evaluated until the sample fracture, measured in

mm. This parameter is called Erichsen Index (EI). Other necessary information within the characterization of IF sheets involved are tensile tests, Hole Expansion tests and  $n$ - $r$  values determination. It is relevant to remember that drawability is the aptitude to develop a good plastic flow in the sheet plane, meanwhile the steel simultaneously presents high resistance to plastic flow in the thickness direction. This mechanical property is called normal anisotropy and it is evaluated by  $r_m$  values or the average of  $r$  [6]. It was possible in this case to calculate  $r_m$  values by the expression (1) that involves  $r$  values determined on samples tested (by tensile test) at  $0^\circ$ ,  $45^\circ$  and  $90^\circ$  respect rolling direction (RD). The planar plastic anisotropy ( $\Delta r$ ) was calculated using the expression (2).

$$r_m = (r_0 + 2r_{45} + r_{90}) / 4 \quad (1)$$

$$\Delta r = (r_0 - 2r_{45} + r_{90}) / 2 \quad (2)$$

where:  $r_m$  - normal anisotropy  
 $\Delta r$  -planar plastic anisotropy

The  $r$  values can also be determined by crystallographic texture of the steel sheet, approximating very well the experimental values [6, 7].

The superplastic flow conditions of this type of steels, are of a mixed nature because of integration of structural and external (experimental variables), which are combined with a mechanical characteristic.

In the industrial practice, plastic deformation processes are limited by the failure of the sheet, which can include: diffuse or global constraint, localized constraint (necking), ductile fracture (tearing), brittle fracture, folds formation, surface roughness and elastic recovery (springback). Necking is determined by the hardening coefficient  $n$ , since it determines the ductility, before the thinning starts. All of them affect the final shape or quality of the product and depends on the material properties. The sheet thickness evolution is relevant related to the states of biaxial tension and less important in pure compression state. The objective of this paper was to discuss the mechanical behaviour considering mechanical resistance, ductility, deep drawing and deformability of the selected IF steel, in correlation with microstructural aspects and deformation mechanisms.

Thermochemistry of the alloys is considered a very important knowledge to understand the complex phase transitions in order to optimize industrial processing conditions and to evaluate the mechanical behaviour [8].

To dispose information of phase transitions and precipitation phenomena on the IF steel, a thermodynamic study was carried out applying a FactSage 8.1 simulation. The calculus was carried out applying Scheil cooling (of non-equilibrium) which provided valuable results that were also correlated with the microstructure characterization information. It is relevant to mention that Scheil cooling simulations also allowed to obtain plots with the amounts of phases versus temperature. The results were corroborated by dilatometric tests carried out at different cooling rates, applying the methodology mentioned in [9].

The fracture surface of the samples subjected to tensile test up to failure, were studied by scanning electron microscopy. Plastic constraint is developed in the necked region when the material achieved the yield strength level. The results make it possible to evaluate localized constraint or necking and ductile fracture or tearing. The knowledge on the strain evolution associated with thickness decrease during deformation, is very useful because the failure in sheet metal forming during rolling or stamping usually occurs by thinning or localized necking. The fracture in the forming process of sheet metal is brought by the superplastic flow behaviour of the material, ductile fracture of metal is

caused by the nucleation, growth, and coalescence of voids or dimples [10].

The information obtained is considered a contribution of interest to the automotive industry since in-depth knowledge of both the material used and the forming process allows lower production costs during the design, development and manufacturing stages of a steel for automotive parts industrial use.

## MATERIAL AND METHODS

The material selected for this study was a commercial 0.8 mm thick Interstitial Free steel sheet. The steel has ultra-low C and N contents (<20 ppm and 47 ppm respectively); and it was stabilized by Ti (510 ppm) and V (30 ppm) additions. The chemical composition of the material is presented in **Table 1**.

**Table 1** Chemical composition of the IF steel in weight %

C	Ti	V	N	S	Mn	P	Cr	Si
0.001	0.05	0.00	0.004	0.001	0.09	0.01	0.00	0.00
5	1	3	7	1	5	8	9	9

The structural characterization of the IF steel was carried out on a sample of the as received material (AR). For this purpose, the observation by optical microscopy (OM) was performed using an Olympus GX51 microscope with the Material Plus image analyzer. The study was completed by scanning electron microscopy (SEM), integrating semi-quantitative chemical analysis (EDS) to evaluate the precipitation phenomenon, using a FEI Quanta 200 equipment. Samples were prepared in high density phenolic resin and were manually polished with SiC abrasive papers from 180 to 1200  $\mu\text{m}$ . Final polishing was carried out with 6  $\mu\text{m}$ , 3  $\mu\text{m}$  and 1  $\mu\text{m}$  diamond paste and cloths. The metallographic attack used to reveal the overall structure is Nital 2%. The structural study also considered the fracture surface observation and the thickness evolution measurements carried out by SEM. Microhardness measurements using a Leco LMT 300 instrument of the steel samples also were carried out.

The thermodynamic simulation was performed by the software Fact Sage 8.1. Different databases were included: FSteel, FMisc, FTOxCN and FSteel. By Scheil cooling calculations (of non-equilibrium), the  $\gamma \rightarrow \alpha$  phase transformation temperature of the steel was determined and corroborated by dilatometric tests, carried out applying a Theta Dilatronics II instrument and considering different cooling rates. In addition, the content (in gram) of each precipitate predicted in the system were determined. The simulation was carried out considering the chemical composition of the IF steel and the temperature range from 100  $^\circ\text{C}$  to 1150  $^\circ\text{C}$ .

The mechanical behavior of the IF steel sheet was determined by different mechanical tests to evaluate the formability behaviour under high deformation. The mechanical properties included tensile strength, yield point, percent of elongation and the values of  $n$  and  $r$ , were determined by tensile tests. The specimens were cut out from the same sheet considering the angles:  $0^\circ$ ,  $45^\circ$  and  $90^\circ$  respect to rolling direction, to proof the anisotropy of the material. The samples dimensions for tensile tests and  $n$ - $r$  determinations are detailed in **Fig. 1**. The uniaxial tensile tests were carried by an Instron 4486 machine with a maximum capacity of 30 t. The strain hardening  $n$ , the plastic strain ratio  $r$  and the planar anisotropy  $\Delta r$ , were considered the conventional indicators of formability of sheet metals.

Erichsen and Hole Expansion tests were performed with a CIFIC machine. The Erichsen Index (EI) was determined from the average of 3 measurements using a hemispherical punch with a diameter of 20 mm and applying a load of 2 t. The Hole Expansion test was carried out using a load of 10 t (corresponding to the maximum possible load for the equipment) and the  $\lambda$  value was

determined by the average of 3 measurements; where  $D_i$  is the initial diameter and  $D_f$  is the final diameter.

$$\lambda = (D_f - D_i / D_i) * 100 \quad (3.)$$

Where:  $\lambda$  - average value of 3 measurements  
 $D_i$  [mm] - initial diameter  
 $D_f$  [mm] - final diameter

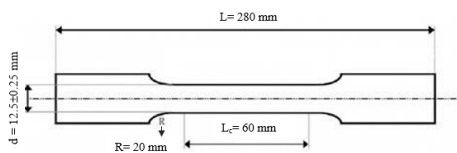


**Fig. 1** Geometry and dimensions of the steel samples used for uniaxial tensile tests and n-r coefficients determination.

## RESULTS AND DISCUSSION

The qualities of steels in terms of their drawability are usually classified in increasing order with the names CQ (Commercial Quality), DQ (Deep Quality), DDQ (Deep Drawing Quality) and EDDQ (Extra Deep Drawing Quality); this last quality corresponds to the IF steel under study. As was mentioned, the requirements of good strength and high formability ability of IF steel, have a high dependence on microstructure and texture. For this reason, in this study a microstructure characterization of the as received material was carried out. The structural evaluation was correlated with the mechanical behaviour determined by different forming aptitude, mechanical tests.

### IF steel structural characterization

Longitudinal and transversal sections samples of the IF steel sheet were observed by optical microscopy. The structure presented equiaxed ferritic grains of ultra-fine size (of G index = 12 to 14, according to the ASTM E 112 standard).

In addition, the equiaxed grains were stabilized and recrystallized during the annealing treatment. The high number of triple points and straight grain boundaries edges corroborated this opinion.

**Fig. 2** shows small precipitates distributed within the ferritic grains and large particles of precipitates present in the grain boundaries, with different morphologies.

According to [11], in which the microstructure texture aspects were deepened, it was verified that the grains in low relief correspond to the so-called grains  $\alpha$  and those that are in over relief correspond to grains  $\gamma$ , the combination of both gives the characteristic texture, of this high formability alloys or suitable for deep drawing.

The study was completed by scanning electron microscopy (SEM) and semi-quantitative EDS analysis, the characteristics of the ferritic grains ( $\alpha$ ,  $\gamma$ ) were corroborated and the distribution and chemical composition of the precipitates present in the material were established. **Fig. 3**.

In the grain boundaries, the presence of cuboid particles  $\sim 5 \mu\text{m}$  in size, which presents a Ti content peak were identified and considered compatibles with TiN. TiC and TiFeP precipitates were also determined. Particularly, TiFeP precipitates which tends to be formed over TiC surface and control the recrystallization and texture of the steel.

In the study, was relevant to consider that different interphases were present in the microstructure: a) between different types of ferritic grains, b) between the ferritic grains and the precipitates and c) between ferritic matrix and small precipitates.

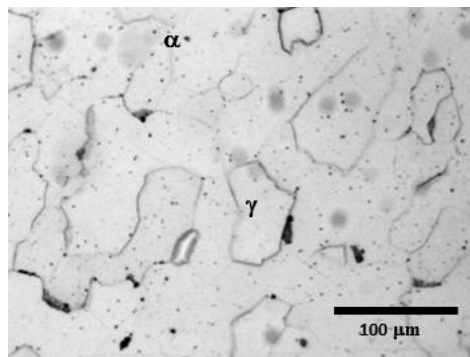


**Fig. 2** Structure with equiaxed ferritic grains (of  $\alpha$  and  $\gamma$  types) and with presence of different precipitates.

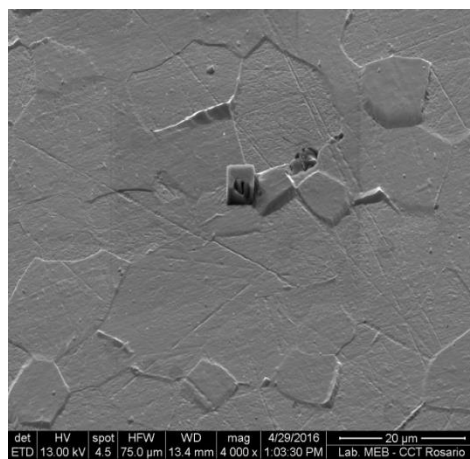


**Fig. 3** Large cubic TiC precipitate present in a ferritic grain boundary and fine precipitates present inner the grains.

In addition,  $\text{C}_2\text{S}_2\text{Ti}_4$  precipitates were identified in the structure associated with triple points. This type of particles improves drawability capacity.

The precipitates identified inside the grains, presented different morphologies and compositions and were considered compatibles with TiN (cubic) and TiS (spherical). Both precipitates (TiN and TiS) improve drawability capacity, without consuming the carbon solute from the matrix.

In this paper through Scheil cooling calculations, phases evolution and distribution in the IF steel was determined applying FactSage 8.1. This cooling simulation provided the transformation temperature value  $T_{\gamma\alpha} = 926^\circ\text{C}$ , associated with  $\gamma(\text{fcc}) \rightarrow \alpha(\text{bcc})$  transformation of this IF steel. **Fig. 4**

The  $T_{\gamma\alpha}$  transformation temperature can be controlled by the Ti content and the cooling rate ( $V_e$ ), during the industrial process.

In order to evaluate the impact of the  $V_e$  on  $T_{\gamma\alpha}$ , dilatometric tests were performed applying cooling rates between 5 to  $0.03^\circ\text{C/s}$ , a similar methodology was used in [9]. The results are visualized in **Fig. 5** and it is possible to observed that at low  $V_e$  ( $-0.03$  to  $-0.025^\circ\text{C/s}$ )  $T_{\gamma\alpha}$  and  $T_{f\gamma\alpha}$  temperatures presented values  $\sim 900^\circ\text{C}$ . However, when  $V_e$  ( $-0.5$  to  $-2^\circ\text{C/s}$ ) both temperatures increased up to  $T_{\gamma\alpha} = 948^\circ\text{C}$  and  $T_{f\gamma\alpha} = 936^\circ\text{C}$ . The increase of the cooling rate up to ( $V_e \geq 2^\circ\text{C/s}$ ) resulted in higher transformation temperature values ( $T_{\gamma\alpha} = 987^\circ\text{C}$  and  $T_{f\gamma\alpha} = 960^\circ\text{C}$ ). This

information allowed to think that with  $V_c$  variation it is possible to control both the  $\gamma(\text{fcc}) \rightarrow \alpha(\text{bcc})$  transformation temperature and the final austenite grain size during the industrial processing. Baker in [12], informed that TiN precipitates volume fraction allows to control the austenite grain size and, in consequence, the final ferritic grain size. In addition, V content increase the ferritic phase strength.

By Scheil cooling simulation, the precipitation evolution with temperature also was obtained, see Fig. 6. The precipitation results were consistent with the information found by SEM + EDS. The results allowed to note that at temperatures higher than  $T_{\gamma\alpha}$  (in austenite phase of the steel) the main precipitate predicted in the structure was the TiN identified as (FCC#2) FCC-A2, however at temperatures lower than  $T_{\gamma\alpha}$  (in ferritic phase) the TiN showed a crystallographic variation denominated as ((FCC#1)FCC-A1. Ooi et al. in [13], also informed consistent results respect TiN precipitation for IF steel at similar temperatures probable associated with the steel solidification or slab reheating.

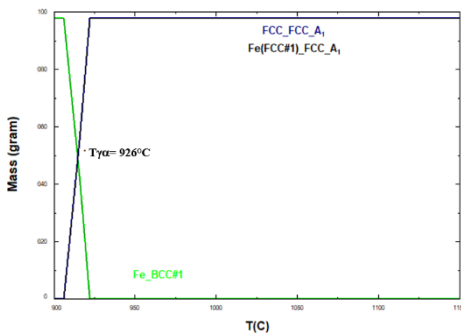


Fig. 4 Transformation temperature ( $T_{\gamma\alpha}$ ) of the IF steel obtained by Scheil cooling calculation.

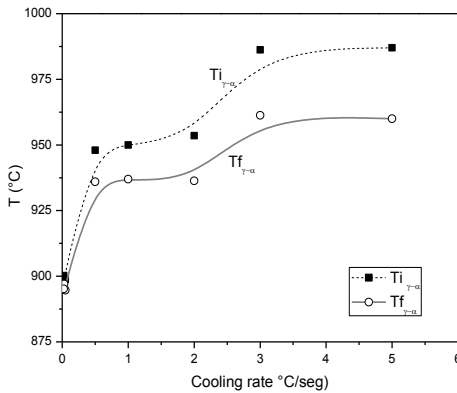


Fig. 5 Cooling rate ( $V_c$ ) effect on the evolution of  $\gamma(\text{fcc}) \rightarrow \alpha(\text{bcc})$  transformation temperatures for the IF steel.

The precipitates such as: TiC, STi and  $\text{C}_2\text{S}_2\text{Ti}_4$  were predicted when the steel is in austenite phase and the maximum proportion in the structure was estimated at  $T_{\gamma\alpha} \leq 926^\circ\text{C}$ . On this base, it was assumed that during the industrial processing, TiN ((FCC#1)FCC-A1, TiC, STi and  $\text{C}_2\text{S}_2\text{Ti}_4$  reach their highest volumetric fraction during coiling process or in the batch annealing treatment, because in both cases the temperatures are lower than  $\gamma(\text{fcc}) \rightarrow \alpha(\text{bcc})$  transformation. The TiC (mainly formed at

$T \leq 926^\circ\text{C}$ ) retards the grain growth associated with {111} texture grains during continuous annealing and promotes a good impact on the r value of the steel. In agreement with [13, 14], the TiC were identified in the IF steel by SEM as spherical particles and TiN as cuboid coarsened particles. The authors in [13, 14], also determined the same shapes for TiC and TiN in the IF steel respect the observed by SEM in this study.

When the precipitation phenomenon is homogeneous, it results in coherent precipitates. The presence of strain fields produce semicoherent and incoherent precipitates, interphase precipitation, heterogeneous precipitation on grain boundaries and in dislocations [15].

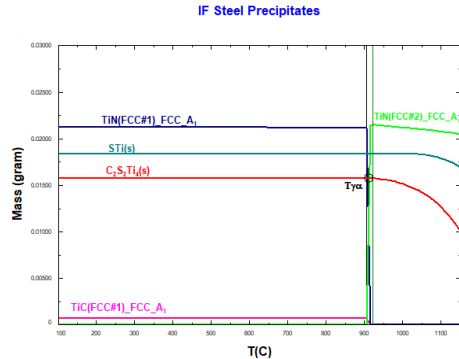


Fig. 6 Precipitates evolution in relation with temperature and phases of the steel predicted by Scheil cooling calculation.

In agreement with Baker in [12], the results obtained (see Fig. 6) showed that the main interphase precipitation occurs during the transformation of austenite to ferrite ( $\gamma(\text{fcc}) \rightarrow \alpha(\text{bcc})$ ). Also, it was observed the efficiency of the Ti addition in the steel to eliminate N, S and C. This element easily forms TiN during casting and TiS during slabs reheating. The major volume fraction of TiS precipitate is achieved at temperatures  $\sim 1000^\circ\text{C}$ . A similar result was obtained by Kuziak et al. in [15], the authors informed that diffusion controls the precipitation of TiC. A low cooling rate promotes epitaxial particles growth on TiN facets surface, however fast cooling promotes individual particles precipitation in the ferrite matrix. Subsequently, the S and N are removed with the remaining Ti which is combined with TiC during the coiling. It is worth mentioning that by means of the cold rolling process a reduction in the thickness of the sheet of the order of 70 - 80% is achieved, until reaching a final thickness of 0.6 - 0.9 mm, such as the IF sheet in study. As the percentage of cold reduction increases, a texture is generated mostly with orientations {111} {100} as was reported in [11].

Particularly, with an important ferrite grain refinement steel strength and toughness also increase. Ferrite grain refinement is obtained through two mechanisms: fine recrystallized austenite grains formed during hot rolling (controlling the soaking stage) at intermediate temperatures and austenite deformation below the recrystallization temperature, which promotes ferrite nucleation in the structure.

#### IF steel formability aptitude characterization

Within the numerous manufacturing processes of industrial products, the metal forming by plastic deformation is one of the most important. By this type of processes auto parts with complex final forms are obtained, from the action of external forces capable of exceeding the elastic limit of the material. Among the

processes applied to sheets, it is possible to mention stamping, stretching and a combination of drawing and bending. One of the most steel used to obtain good formability of automotive parts is the IF steel. In this type of steel, one of the most relevant problem in the design and analysis of sheet drawability aptitude is the fracture prediction. If the steel sheet does not present a good mechanical behaviour, fail could cause a ductile fracture surface during the forming process in the industry.

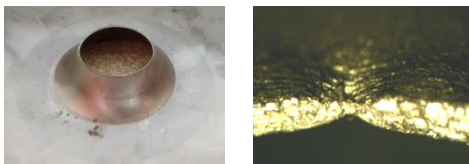
In this study different mechanical tests were carried out to evaluate the drawability aptitude of the IF steel sheet: Erichsen stretching tests (to obtain the Erichsen Index), Hole Expansion tests, tensile tests on samples cutted at 0°, 45° and 90° (respect RD) for n and r values determination, were carried out. The normal (r) and planar ( $\Delta r$ ) plastic anisotropy coefficients have been calculated by applying eq. (1) and (2), respectively.

Erichsen cupping test for IF steel sheet was carried out placing the sample in the machine and punching a cup into the sheet until a crack appearance. Then the depth of the cup was measured, and the ductility was determined as a function of the length of penetration in mm. The value indicated the EI number which provided the ductility behaviour in the drawing plane under biaxial stress conditions [16].

To obtain the Erichsen index (EI) values, 3 imprints were made on samples of the IF sheet, at 60 mm from the sheet edge and separated 90 mm one from each other. The deformation was provided by the hemispherical punch, applying a load of 2 t. The index obtained was EI = 12.7 mm (of depth of deformation), in all cases normal breaks were generated. The EI value obtained allowed to consider that the IF steel sheet presented a good ductility under biaxial deformation efforts.

Hole Expansion test also provided relevant information of the steel sheets [17]. During this procedure a hole is stretched to increase its diameter, these flanging operations stretch the material, that previously has already been subjected to certain plastic deformation during hole preparation. In this case, samples with circular holes of 10 mm diameter were prepared. The test was performed using the maximum load of the machine (10 t). After deformation, each of the final hole diameters were measured 3 times and the average value of each test was provided. Finally, the value of  $\lambda$  was calculated applying eq. (3). Hole expansion test results were detailed in Table 2.

After the tests samples were observed by a stereoscopic magnifying glass to verify the hole surface appearance. Only sample 3, presented a localized thickness decrease (not normal, necking), however without fissure. The authors in [17], mentioned that imperfections and damage introduced during sample preparation in the vicinity of the hole could cause a detrimental influence on the hole expansion property and decrease material formability. Fig. 7 shows both aspects after hole expansion test (with "good" and "failed" results observed in the hole surface).



a) Good aspect of hole surface. b) Failed aspect with necking presence of sample 3.

Fig. 7 Aspects of the samples after hole expansion test results (a) good, (b) failed.

Kim et al. in [18] established that the material microstructure is strongly sensitive to the hole expansion formability of steel

sheets and allows to evaluate the stretchability by the hole expansion ratio ( $\lambda$ ) measurement. The good ratio value obtained for the IF steel sheet is consistent with the microstructure results obtained.

Table 2 Results of the Hole Expansion tests of the IF steel sheet.

Sample	Result	Load (t)	D <sub>r</sub> (mm)	D <sub>F</sub> average (mm)	$\lambda$ (%)
1	good	10	10	23.18	131.8
2	good	10	10	23.22	132.2
3	failed	10	10	23.19	131.9
$\lambda$ average (%)					131.9

The results of the tensile tests carried out on the samples at 0° (L1), 45° (D1) and 90° (T1) with respect to the rolling direction (RD), are presented in Table 3. Yield limit presents values in the characteristic range 140-150 MPa of the IF steels. Furthermore, the ER values obtained from the R<sub>0.2</sub>/R ratio can be observed in the same table.

It is important to mention that ER values correspond to the elastic relationship that establish the material aptitude for stamping pieces. The mechanical behaviour were consistent with the fine grain size measured, the presence of  $\alpha$  and  $\gamma$  grains associated with texture, the steel microhardness value obtained (H<sub>v</sub> ~ 114) and the precipitates identified in the microstructure.

In Figure 8, the comparison of the tensile test curves for all the angles tested of the IF sheet is presented.

Table 3 Tensile tests result of the IF steel sheet.

Sample	Tensile strength (MPa)	Yield limit (R <sub>0.2</sub> ) (MPa)	Elongation (E) (%)	ER
0° (L1)	303.9	143.6	44.1	0.47
45° (D1)	294.9	141.9	43.1	0.48
90° (T1)	275.8	133.1	43.5	0.48

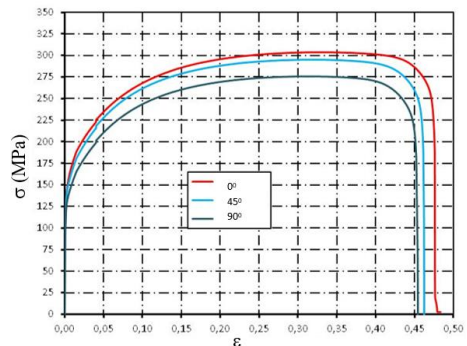


Fig. 8 Comparison of the tensile test's curves of samples at angles 0°, 45° and 90°, respect RD.

Due to the characteristics and variables of the rolling process that affect the microstructure evolution, sheets generally exhibit significant anisotropy of the mechanical properties.

The variation of the plastic behaviour as a function of the direction is evaluated by the anisotropy coefficient or Lankford coefficient "r" (determined by uniaxial tensile test and defined by the ratio of the deformation in width and thickness,  $r = \epsilon_2/\epsilon_3$ ). Since the thickness is much less than the width and length of the sample, only the length and width are considered when determining

the r-value ( $\epsilon_1 / \epsilon_2$ , where  $r = \epsilon_1 / (\epsilon_1 + \epsilon_2)$ ). The r value is associated with the planar anisotropy of the steel sheet. In deep-drawing operations, both normal as well as planar anisotropy need to be considered to design process parameters. Another important parameter is “n” which the hardening coefficient of the steel is during deformation.

The comparison of the IF sheet tensile curves (Figure 8) shows that the material in the three directions presented a similar behaviour. As was expected, the sample L1 (0° with respect to RD) was the one with the highest deformation capacity and T1 (90° with respect to RD) developed the least possibility of deformation respect to the others. However, this fact shows that the sheet has a good drawing anisotropic behaviour. In Figure 9 (a) and (b), the curves obtained in the tests for the determination of n, r and  $\Delta r$ , corresponding to the IF sheet samples (L2, D2, T2 and L3, D3, T3), are presented. In both cases the curves obtained at 45° and 90° are practically overlapped in the elastic and plastic deformation behaviours. In agreement with [19], the higher the normal anisotropy and the lower the planar anisotropy, the better is considered the sheet for forming operation applications. In Table 4, the values of n (hardening coefficient), r (normal plastic anisotropy coefficient),  $r_m$  (average normal plastic anisotropy coefficient) and  $\Delta r$  (planar plastic anisotropy coefficient) obtained can be observed.

The deep drawability of the IF steel strip was influenced by the crystallographic texture of the steel. This opinion was consistent with the higher volume fraction of  $\gamma$  fiber grains identified in the microstructure that are associated with {111} planes texture as result of the rolling plane [19].

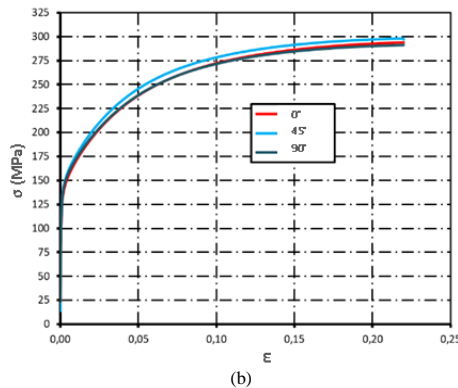
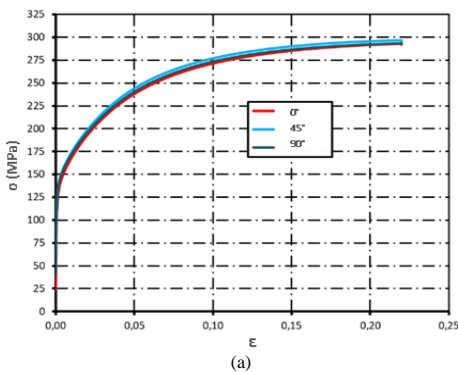


Fig. 9 Tensile curves used for n, r and  $\Delta r$  of the IF sheet. (a) samples L2, D2, T2, (b) samples L3, D3, T3.

In addition, the results obtained associated with precipitates formed in this ultra-low C steel with Ti additions, contributed to developed a very low elastic limit (less than 150 MPa), which allowed to predict that the material satisfied the requirements to produce final shapes with small efforts.

The material also presented low yield point (YS), high uniaxial elongation (E%), high coefficient of plastic anisotropy r or Lankford coefficient ( $\geq 1.8$ ) promoting a good drawability.

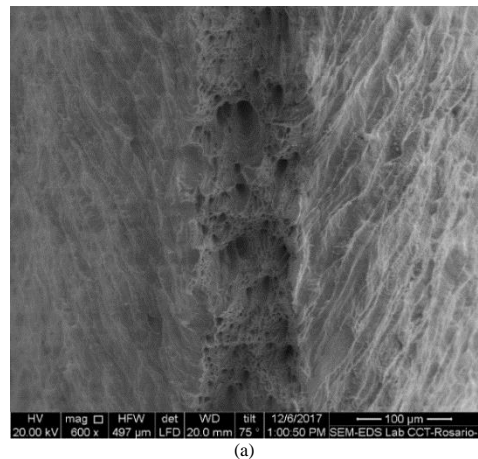
The high exponent of strain hardening  $n \geq 0.22$ , which measured the ductility, corroborated non-striction risk and strain-aging resistance [5].

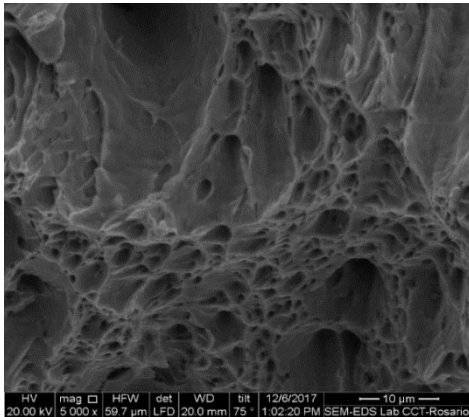
Table 4 Results of RE, n, r,  $r_m$  and  $\Delta r$  obtained for the IF sheet.

Sample	Strain range (%)	n	r	$r_m$	$\Delta r$
L2(0°)	22	0.26	1.93	1.92	0.17
D2(45°)	22	0.25	1.84		
T2(90°)	22	0.25	2.09		
L3(0°)	22	0.26	1.75	1.91	0.37
D3(45°)	22	0.25	1.73		
T3(90°)	22	0.25	2.40		

Fractography study of the sample tested up to rupture.

The study was carried out on the fracture surface of the sample subjected to tensile test up to failure. The observations were made by a stereoscopic magnifying glass and scanning electron microscopy (SEM), using different magnifications. Both observations allowed to note that the fracture surface showed characteristics of a ductile fracture, corroborated by a large presence of dimples or holes with different sizes which indicates a high ductility of the material. The fracture mechanism identified is associated with dimples nucleation, growth and coalescence, in the plane of maximum tangential stress, see Figure 10 (a) and (b). Particularly, Figure 10 (a) shows the aspect of the both sheet surfaces with clear deformation presence (near the necking zone) and the fracture surface which presented small and large dimples distributed. At higher magnification (Figure 10(b)) it was corroborated that small dimples were integrated with larger dimples (larger dimples were formed through coalescence micro-mechanism). However, in agreement with [9], it is relevant to mention that the ductile fracture criteria change for different strain conditions applied during tensile tests (uniaxial) and Hole Expansion test (triaxial).





(b)

**Fig. 10** Fracture surface of the sample subjected to tensile failure, which evidence high plastic deformation.

Some cavities (dimples) could be present in the steel as result of the previous rolling process, however they could also had nucleated in grain boundaries because of insufficient accommodation or sliding. Triple points and hard precipitates enhance the nucleation of these cavities. The individual cavities growth (up to a critical size,  $r_c$ ) during deformation and when two cavities meets merge into one cavity with a larger volume. The critical radius  $r_c$  of the cavity depends on the surface tension and the tensile stress. The measurements carried out on the fracture surface by SEM (**Figure 10** (b)) showed that the major quantities of cavities presented a critical radius  $r_c \sim 21 \mu\text{m}$ , also part of the cavities presented medium values  $r_c \sim 47 \mu\text{m}$  and the larger cavities presented  $r_c \sim 70 \mu\text{m}$ . The fractography study corroborated the ductility behaviour of the IF sheet and a large plastic deformation capacity prior failure.

#### Sheet thickness profile evolution during necking of the IF steel

The evolution of the sheet thickness profile generated during the period of necking until failure was measured by SEM. Ten measurements of thickness were carried out in areas far from the failure ( $Z_f$ ) and ten measurements were carried out in areas with necking ( $Z_n$ , close to the fracture). The results allowed to evaluate the thickness decrease occurred during the necking period until failure. The longitudinal measurements were made considering distances of  $181.6 \mu\text{m}$  between each other. In **Figure 11**, the average thickness of the steel sheet in the area far from failure ( $E_{\text{max}} = 630.7 \mu\text{m}$ ) assumed as the original IF sheet thickness is observed. However, the thickness measurements carried out in the necking zone of the sample allowed to established that during the necking period (until failure) an important sheet thickness decrease had occurred (showed by  $E_{\text{min}} = 254.20 \mu\text{m}$ ) and was assumed as  $\sim 40.30\%$  of thickness reduction. The results verified the presence of a progressive and unstable thinning of the IF sample material until the tear, when the break occurs. This constitutes the usual failure of ductile materials, with the presence of important necking and ductile fracture (tearing). The influence of thickness is high for biaxial tensile states and decreases up to fade when the material is subjected to pure compression. Understanding the formability of the sheets is essential to achieve high quality in the production of parts by stamping [20]. As it is known, the IF steel with very fine grains develops ultrahigh strength at the expense of ductility.

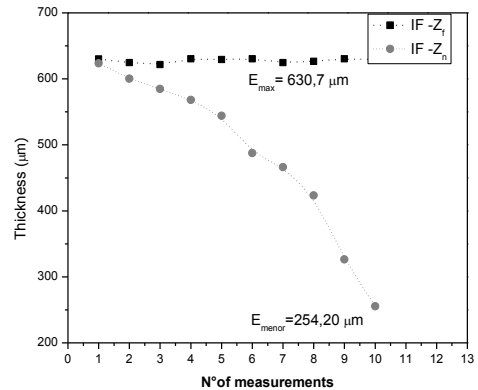


**Fig. 11** IF steel sheet thickness evolution during necking measured by SEM.

#### Thinning of the IF steel sheet.

During the large deformation in the industrial processes of rolling and stamping, significant thinning of the sheet could occur. It is relevant to consider that this thinning may not be uniform throughout the sheet. In the industry dimension requirements of the products constitutes a quality proof, for this reason the thinning behaviour must be studied and understood in order to improve the design and production of automotive parts.

Non-uniform deformation could occur promoting necking and thinning, under uniaxial tension or circular sheet bulging process. In this sense, the thinning behaviour (associated with superplastic flow) must be studied and understood in order to improve the design and industrial production of IF steel automotive parts.

Superplasticity is the ability of a polycrystalline material to exhibit (generally as isotropic manner) very high tensile elongation prior to failure.

The structural superplasticity is habitual in steels with very stable and fine grain size in which the average grain size should not exceed  $10\text{--}15 \mu\text{m}$ . This information is in complete agreement with the G index  $\sim 12$  to  $14 \mu\text{m}$  obtained in the IF sheet grain size measurements performed.

Superplastic steels are able to experiment large amounts of uniform deformation controlled by different mechanisms acting in the microstructure, such as stress induced by vacancy migration, dislocation climb associated with glide and grain boundary sliding (GBS, related to interphases conditions).

Commonly, during the deformation process, the mentioned mechanisms acts together (not as individual mechanisms). Grain boundaries sliding (GBS) cannot occur on all of them without some deformation presence within themselves, because they are affected by lattice defects and the inner precipitates present (TiN, TiS), considering the coherency level of them with the ferritic matrix. It is possible to consider that GBS in the IF steel studied was also affected by the interphase nature between the  $\alpha$  and  $\gamma$  grains identified in the structure. In addition, the diffusion along grain boundaries promoted the accommodation mechanism which enhanced elements transference across the grain interphases and triple points, promoting the precipitates formation:  $\text{C}_2\text{S}_2\text{Ti}_4$  (at triple points), TiN (cubic) and TiFeP precipitate identified on the surface of TiC particles. In triple points, GBS mechanisms become more complex.

Along the years, there has been a large debate about the mechanisms responsible of materials superplastic behaviour. During plastic deformation, polycrystalline materials present different phenomena that includes nucleation, propagation and interaction

of punctual defects (vacancies, impurity atoms), linear defects (dislocations), planar surfaces (grain boundaries, interfacial boundaries) and volumetric phenomenon (cracks, pores) present in the structure [21-27]. Different authors [22-25], proposed that the main deformation mechanism in the superplasticity is the grain boundary sliding (GBS), controlled by dislocations motion (within the grains). Dislocations can travel along the most favorable slip plane within the blocked grains and pile-up at the opposite grain boundary. In this case the intragranular deformation was assumed as an accommodation process which accompanied the grain boundary sliding. In addition, the substructure evolution in the grain and the interphases between the matrix with inner precipitates also affected.

Recently, new concepts which involve the mesolevel of superplastic deformation were introduced and which consider that grain boundary sliding does not take place independently on the interfaces of the polycrystalline material, because also include (in a single process) the presence of shear efforts in the grain boundaries [21]. In this IF steel was considered that the presence of precipitates in grain boundaries (such as TiC, TiFeP) and the interphases nature also were contributed to control the superplastic behaviour.

The stability of the superplastic deformation allowed avoiding thinning or necking in the sheet. A stable flow pattern formed cooperative grain boundary sliding, probably (CGBS) bands, which ensured the maximum homogeneity of deformation [21]. However, different causes induced the material instability and structure damage accumulation: strain hardening and strain rate hardening [24].

The instability of the deformation caused the start to failure and it was regarded as the beginning of the neck formation in the specimen, that means a localized deformation in some cross-section (irreversible growth of the neck) and the sheet thickness decrease, also was started. However, the thickness measurements carried out in the sample tested up to rupture, showed that during the instable deformation the IF sheet support a high plastic deformation (see, **Figure 11**).

It has been found that instable superplastic deformation was accompanied by the cavitation phenomenon, that involved mechanisms such as: cavities growth by plastic deformation associated with GBS and the probable vacancy diffusion. The GBS constituted the main mechanism acting during superplastic deformation. Cavity growth was controlled by the IF steel plasticity, which gave cavity growth through a combination of bulk deformation and GBS effects. In addition, precipitates presence (in the grain boundaries) contributed to the cavity formation. The mechanism proposed is described in **Figure 12** and was consistent with the model of cavity nucleation mentioned in the review carried out by X.G. Jiang et al. in [26].

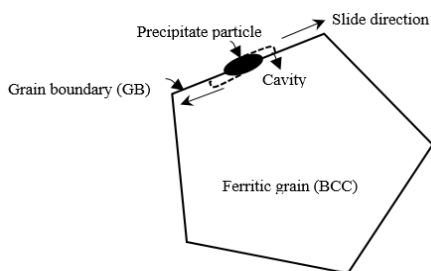


**Fig. 12** Cavity mechanism formation proposed for the IF steel sheet.

The precipitates particles (such as TiC, TiFeP and TiS) promoted the cavities nucleation, growth and interlinkage according

with the particular interphase nature conditions (including surface tension  $\gamma$  behaviour) of each particle type and the ferritic grain boundary slide (GBS) effect. The  $r_c$  different values of the cavities obtained by SEM microscopy together with the deformation stress condition, corroborated the presence of the mentioned mechanism.

During the superplastic deformation, cavities also were nucleated in grain boundaries defects, triple points or preexistent microvoids (formed during rolling process), due to stress concentration.

This cavitation process was assumed as the degradation mechanism that induced the fracture in the material. Cavity growth and interlinkage was predominant before fracture development and external thinning, in agreement with [20-25]. The cavities interlinkage occurred along a direction parallel to the tensile stress, before failure of the sample.

On this base, the control of cavitation process of the material produced by multiples sites of nucleation including the precipitate types, their crystalline characteristics (including the interphase nature with the matrix) and their volume fraction was considered one of the most important feature to guaranty the production level of automotive parts with the IF steel. This purpose is aligned with the current research carried out as result of the demand of high-performance lightweight materials with good toughness, strength and formability from the automotive industry that involves to establish the better processing thermomechanical parameters in the steel-making industry [28-32].

## CONCLUSIONS

In this paper the drawability aptitude of the IF steel was determined by mechanical tests. The results obtained were corroborated by microstructural observations, the thinning behaviour associated with necking and by fractography study. The steel presented a behaviour suitable for the EDDQ quality (Extra Deep Drawing Quality), showing its total suitability for applications in automotive panels. This opinion is justified by the information obtained through the Erichsen tests (with an average of IE = 12.7 mm), the Hole Expansion tests that indicate a  $\lambda > 132\%$  (without the presence of any cracks) and the values of n and r coefficients. It was verified that the  $r_m$  values were 1.91 and 1.92 (higher than the necessary minimum of 1.8), the planar plastic anisotropy  $\Delta r$ , resulted in values 0.17 and 0.34 (considered acceptable because of the ideal value for this type of steels should be 0) and the n coefficients (0.251 and 0.260, higher than the required minimum of 0.220). The structural study was in complete agreement with the good mechanical behaviour (drawability aptitude) obtained. The IF steel sheet presented a ferritic structure with equiaxed ultra-fine (G index=12 to 14) and stabilized grains (during annealing treatment). The microhardness value determined was ( $H_v \sim 114$ ) was compatible with the mechanical behaviour obtained. It was also demonstrated that the proportion of  $\alpha$  and  $\gamma$  fibers provided the appropriate texture for the good formability aptitude of the material. In addition, the structure presented precipitates distributed within the grains and on the grain boundaries. The main precipitates identified were TiN and TiS (within the grains) and  $C_2S_2Ti_4$  (on triple points), all of them improve steel strength and formability properties. This condition is also enhanced by the presence of precipitates on grain edges such as: TiC (cubic) of size  $\sim 5 \mu m$  and TiFeP (larger), which impact on the recrystallization and the texture of the steel. The precipitates identified by microscopy and EDS analysis were consistent with the Scheil cooling predictions, carried out by FactSage 8.1. This information allowed to understand the structure evolution in relation with temperature, considering both phases and precipitates. Furthermore, it was determined that the transformation temperature  $\gamma(fcc) \rightarrow \alpha(bcc)$  of this IF steel sheet was  $T = 926^\circ C$ , which was corroborated by a dilatometry test. The volumetric

fraction of the precipitates was determined and it was possible to verify that TiN and  $C_4Ti_2S_2$ , increases mainly at temperatures lower than  $926^\circ C$ , that means when the steel is in ferritic phase, during cooling stages (of rolling, coiling or post annealing heat treatment). The fractography study demonstrated that the IF steel sheet presented after a great plastic deformation a high ductility fracture behavior, verifying the presence of the superplasticity phenomenon and cavitation mechanism produced during thinning and necking up to rupture. The thinning and necking involved: nucleation, growth and coalesce of voids (dimples). Cavities were nucleated in grain boundaries sites with variable interphases nature, promoted by the interaction between the ferritic grains types ( $\alpha$  and  $\gamma$ ) in contact with: different types of precipitates, triple points, lattice defects and preexistent voids. The cavitation was assisted by the grain boundary slide (GBS). The sample thickness evolution measurements carried out in the sample tested up to rupture, allowed to established that during necking the sheet experimented a reduction of  $\sim 40.30\%$ , going from a thickness  $E_{max} = 630.7 \mu m$  (original sheet thickness) to  $E_{min} = 254.20 \mu m$ , the information was in agreement with the high percentage elongation, the low hardening coefficient  $n$  and consistent with the ductility determined by the EI index obtained by Erichsen test. The study provided information to identify the main factors or process conditions to avoid tearing or dimensions variation that could affect the production level during IF steel auto parts forming.

**Acknowledgments:** Authors are grateful for the financial support for the research to the Universidad Tecnológica Nacional from Argentina.

#### REFERENCES

1. A.H. Bui, H. Le: Acta Metallurgica Slovaca, 22(1), 2016, 35-43. <https://doi.org/10.12776/ams.v22i1.690>.
2. A. Di Schino, P. E. Di Nunzio, J. M. Cabrera: Advanced Materials Letters, 8, 2017, 641-651. <https://doi.org/10.5185/amllett.2017.1487>.
3. R. Unnikrishnan, A. Kumar, R. K. Khatirkar, S. K. Shekhawat, S. G. Sapate: Materials Chemistry and Physics, 183, 2016, 339-348. <https://doi.org/10.1016/j.matchemphys.2016.08.037>.
4. Y. G. Ko, J. S. Lee and Loorentz: Materials Science and Technology, 29, 2013, 553-558. <https://doi.org/10.1179/1743284712Y.0000000189>.
5. M. Romanyuk, M. Avalos, E.R. Benavidez, E. Brandaleze: Advanced Materials Proceedings, 3, 2018, 408-413. <https://doi.org/10.5185/amp.2018/916>.
6. R.K. Ray, J.J. Jonas: International Materials Reviews, 39, 1994, 129-172. <http://hdl.handle.net/11336/93734>.
7. D. Banabic, M. Bos: Annals of the CIRP, 56, 2007, 249-252. <https://doi.org/10.1016/j.cirp.2007.05.058>.
8. I.H. Jung, Z. Zhu, J. Kim, J. Wang, P. Chartrand, A. Pelton: Minerals, Metals and Materials Society, 69, 2017, 1052-1059. <https://doi.org/10.1007/s11837-017-2331-9>.
9. P. Prislupčák, T. Kvačák, J. Bidulská, P. Záhumenský, V. Homolová, P. Zimovčák: Acta Metallurgica Slovaca, 27 (4), 2021, 207-209. <https://doi.org/10.36547/ams.27.4.1306>.
10. Z. Yang, C. Zhao, G. Dong, Z. Chen, Y. Sun, X. Jia: International Journal of Material Forming, 2021, 341-359. <https://doi.org/10.1007/s12289-019-01528-w>.
11. M.Z. Qadir, B.J. Duggan: Acta Materialia, 52, 2004, 4011-4021. <https://doi.org/10.1016/j.actamat.2004.05.017>.
12. T.N. Baker: Ironmaking and Steelmaking, 2015, 1-44. <https://doi.org/10.1179/1743281215Y.0000000063>.
13. S.W. Ooi, G. Fourlaris: Materials Characterization, 56, 2006, 214 - 226. <https://doi.org/10.1016/j.matchar.2005.11.010>.
14. R. Mendoza, M. Alanis, O. Alvarez-Fregoso, J.A. Juarez-Islas: Scripta materialia, 43, 2000, 771-775. [https://doi.org/10.1016/S1359-6462\(00\)00486-3](https://doi.org/10.1016/S1359-6462(00)00486-3).
15. R. Kuziak, H. Hartman, M. Budach, R. Kawalla: Materials Science Forum, 500-501, 2005, 687-694. <https://doi.org/10.4028/www.scientific.net/MSF.500-501.687>.
16. A. Talapatra, V.R. Choudhary, K. Malhotra, M. Vyas, A. Jamal, M.K. Singhi: i-manager's Journal on Material Science, 1, 2013, 14-18. <https://doi.org/10.26634/jms.1.1.2280>.
17. M. Dünckelmeyer, A. Kerova, C. Krempaszy, E. Werner: In: *Proceeding of international doctoral seminar*, Bratislava, 2009, 50-57.
18. J.J. Kim, Q.T. Pham, Y.S. Kim: International Journal of Mechanical Sciences, 191, 2021, 106067. <https://doi.org/10.1016/j.ijmecsci.2020.106067>.
19. P. Ghosh and R.K. Ray, Deep drawable steels, In: *Automotive Steels*, Ch.5, 2017, 113-143. <https://doi.org/10.1016/B978-0-08-100638-2.00005-5>.
20. D.R. Kumar: Journal of Materials Processing Technology, 130-131, 2002, 31-41. [https://doi.org/10.1016/S0924-0136\(02\)00789-6](https://doi.org/10.1016/S0924-0136(02)00789-6).
21. A. Zhilyaev, A. Pshenichnyuk: *Superplasticity and Grain Boundaries in ultrafine grained materials*, Cambridge, Woodhead Publishing 2011.
22. A.K. Mukherjee: Materials Science and Engineering, 8, 1971, 83-89. [https://doi.org/10.1016/0025-5416\(71\)90085-1](https://doi.org/10.1016/0025-5416(71)90085-1).
23. R.W. Hertzberg: *Deformation and Fracture Mechanics of Engineering materials*, John Willey & Sons Inc., Hoboken, USA, 1996, 175-178.
24. K.A. Padmanabhan, R.A. Vasin, F.U. Enikeev: *Superplastic Flow: Phenomenology and Mechanics*, Springer-Verlag Berlin Heidelberg New York, 2001, 149-188.
25. D.J. Zhou, J. Lian, M. Suery: Materials Science and Technology, 4, 1988, 348-353. <https://doi.org/10.1179/026708388790331573>.
26. X. Jiang, J.C. Earthman, F.A. Mohamed: Journal of Materials Science, 29, 1994, 5499-5514. <https://doi.org/10.1007/BF00349941>.
27. T. Kvačák, J. Bidulská, R. Bidulský: Materials, 14(8), 2021, 1988. <https://doi.org/10.3390/ma14081988>.
28. R. Kuziak, R. Kawalla, S. Waengler: Archives of Civil and Mechanical Engineering, 8(2), 2008, 103-117. [https://doi.org/10.1016/s1644-9665\(12\)60197-6](https://doi.org/10.1016/s1644-9665(12)60197-6).
29. J. Zhao, Z. Jiang: Progress in Materials Science, 94, 2018, 174-242. <https://doi.org/10.1016/j.pmatsci.2018.01.006>.
30. S. Hoile: Materials Science and Technology, 16(10), 2000, 1079-1093. <https://doi.org/10.1179/026708300101506902>.
31. L. Xing, J. Guo, X. Li, Z. Zhanga, M. Wanga, Y. Bao: Materials Today Communications, 25, 2020, 101292. <https://doi.org/10.1016/j.mtcomm.2020.101292>.
32. R. Yoda, K. Shibata, T. Morimitsu, D. Terada, N. Tsujia: Scripta Materialia, 65, 2011, 175-178. <https://doi.org/10.1016/j.scriptamat.2011.02.002>.